# Exploring the proton pump mechanism of cytochrome *c* oxidase in real time

**Ilya Belevich, Dmitry A. Bloch, Nikolai Belevich, Mårten Wikström, and Michael I. Verkhovsky***

Helsinki Bioenergetics Group, Program for Structural Biology and Biophysics, Institute of Biotechnology, University of Helsinki, P.O. Box 65, FI-00014, Helsinki, Finland

Edited by Harry B. Gray, California Institute of Technology, Pasadena, CA, and approved December 18, 2006 (received for review October 4, 2006)

**Cytochrome *c* oxidase catalyzes most of the biological oxygen consumption on Earth, a process responsible for energy supply in aerobic organisms. This remarkable membrane-bound enzyme also converts free energy from $O_2$ reduction to an electrochemical proton gradient by functioning as a redox-linked proton pump. Although the structures of several oxidases are known, the molecular mechanism of redox-linked proton translocation has remained elusive. Here, correlated internal electron and proton transfer reactions were tracked in real time by spectroscopic and electrometric techniques after laser-activated electron injection into the oxidized enzyme. The observed kinetics establish the long-sought reaction sequence of the proton pump mechanism and describe some of its thermodynamic properties. The 10-$\mu$s electron transfer to heme *a* raises the $pK_a$ of a ''pump site,'' which is loaded by a proton from the inside of the membrane in 150 $\mu$s. This loading increases the redox potentials of both hemes *a* and $a_3$, which allows electron equilibration between them at the same rate. Then, in 0.8 ms, another proton is transferred from the inside to the heme $a_3/Cu_B$ center, and the electron is transferred to $Cu_B$. Finally, in 2.6 ms, the preloaded proton is released from the pump site to the opposite side of the membrane.**

cytochrome oxidase | electron transfer | proton translocation

Electrochemical proton gradients across phospholipid membranes are generated in primary biological energy transduction, whether powered by sunlight (photosynthesis) or by oxidation of hydrogenated foodstuffs by $O_2$ (respiration). In both cases the proton gradient is then used to synthesize adenosine triphosphate (ATP), the universal energy currency in cellular processes. $O_2$ consumption is usually catalyzed by cytochrome *c* oxidase (CcO), the terminal member of the respiratory chain in mitochondria and many bacteria. Electrons from cytochrome *c* on the positively charged P-side of the membrane are transferred, one at a time, to the binuclear heme/copper ($a_3/Cu_B$) oxygen reduction site located ≈1/3 into the membrane domain (Fig. 1). The electron transfer takes a specific route via the bimetallic $Cu_A$ center at the membrane surface, and another heme group (heme *a*) next to the $a_3/Cu_B$ site (for reviews, see refs. 1 and 2). Because reduction of $O_2$ to water requires four electrons, there are four such one-electron transfers in the catalytic cycle. Each of these is associated with uptake of a substrate proton into the $a_3/Cu_B$ site from the negatively charged N-side of the membrane to form the equivalent of water, and with translocation (pumping) of another proton across the membrane (3). Proton uptake from the N-side takes place via two pathways (Fig. 1) that are differently engaged in subsequent parts of the catalytic cycle (1). Each of the four electron transfer steps in the catalytic cycle of CcO constitutes one cycle of the proton pump, which is likely to occur by essentially the same mechanism each time. Here, we report on the internal electron transfer and charge translocation kinetics of one such cycle, which is set forth by fast photoinjection of a single electron into the oxidized enzyme.

## Results

Photoactivated electron delivery using ruthenium bispyridyl (RubiPy) is a very useful method (4) for studying the reactions associated with transfer of a single electron through CcO (3, 5–7), which is coupled to one of the four proton-pumping steps of the catalytic cycle. The trajectory of the injected electron may be monitored by time-resolved optical spectroscopy, which reveals the redox states of the metal centers. Vectorial proton movements can be tracked in phospholipid vesicles inlaid with CcO by capacitatively coupled time-resolved electrometry (3, 6–9), which is a sensitive method of detecting charge movements within the dielectric of the enzyme structure as long as they are orientated perpendicular to the membrane. These charge movements are mainly due to proton transfers from the N- toward the P-side (Fig. 1), with only a small contribution from electron transfer between $Cu_A$ and heme *a*. Further electron transfer from heme *a* to the $a_3/Cu_B$ site yields no electrometric signal because it occurs parallel to the membrane (10). Consequently, monitoring both electron transfers and proton (charge) translocation in real time can yield valuable mechanistic and thermodynamic insight into the molecular machinery of proton-pumping by CcO.

**Electron Transfer.** Fig. 2*A* shows the electron transfer kinetics after a laser pulse that converts RubiPy into a strong reductant that injects an electron into CcO (4–7). The quantum efficiency is 10–20% in our conditions, which assures, in practice, that either one or no electron is injected. Because of the short time during which the reaction is monitored (a few milliseconds), we can also exclude electron transfer between CcO molecules, which occurs on a much longer time scale (6). Just before the laser pulse the enzyme was reduced and then reoxidized by $O_2$ (11, 12), which is essential, because otherwise the oxidized enzyme is in a ''resting'' state incapable of fast proton-coupled electron transfer (3, 13). Upon excitation, the $Cu_A$ site is reduced first with a time constant ($\tau$) of $<0.5$ $\mu$s (the life-time of the excited state of RubiPy), followed by electron equilibration between $Cu_A$ and heme *a* ($\tau \approx 10$ $\mu$s), where ≈70% of the electron is transferred to the latter (Figs. 2*A* and 3*A*). We emphasize that our methodology yields a full spectrum for each time point, and does not rely on the kinetics at a single wavelength (see *Materials and Methods*), which increases the accuracy of assigning the spectral changes to specific redox centers. The observed noise has a standard deviation of ≈2% of the total redox change of heme *a*, and ≈5% of $Cu_A$.

From the $Cu_A$/heme *a* equilibrium position after the 10-$\mu$s phase

Author contributions: M.W. and M.I.V. designed research; I.B. and D.A.B. performed research; N.B. contributed new reagents/analytic tools; I.B., D.A.B., M.W., and M.I.V. analyzed data; and M.W. and M.I.V. wrote the paper.

The authors declare no conflict of interest.

This article is a PNAS direct submission.

Freely available online through the PNAS open access option.

Abbreviations: CcO, cytochrome *c* oxidase; DM, dodecyl L-D-maltoside; RubiPy, ruthenium bispyridyl.

*To whom correspondence should be addressed at: Institute of Biotechnology, University of Helsinki, Biocenter 3, P.O. Box 65, Viikinkaari 1, FI–00014, Helsinki, Finland. E-mail: michael.verkhovsky@helsinki.fi.

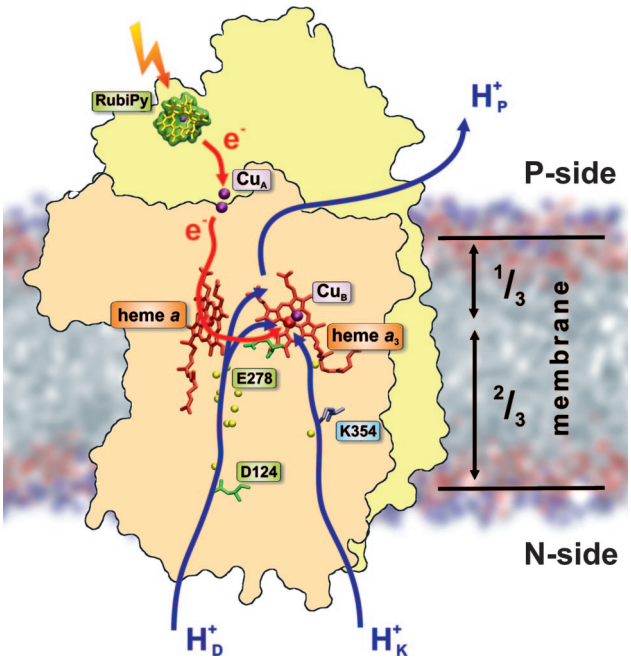


**Fig. 1.** CcO structure and function. The two key subunits, I (pink) and II (yellow), are depicted in the membrane together with the four redox-active centers, $Cu_A$, heme *a*, heme $a_3$, and $Cu_B$. In this work, the reaction is initiated by photoinduced electron injection from ruthenium bispyridyl (RubiPy). The electron transfer path is indicated in red. Proton transfer from the N-side of the membrane takes place via two pathways, D and K (blue arrows; see text). The pumped proton is released to the P-side from an as-yet-unidentified pump site above heme $a_3$. The figure was made with the help of the crystal structure with Protein Data Bank ID code 1v54 (37) and the program VMD (45).

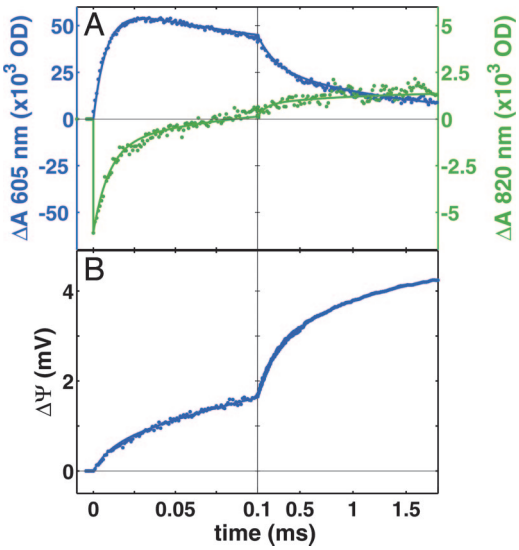


**Fig. 2.** Electron and proton transfer kinetics in CcO. (*A*) The redox kinetics of heme *a* (blue, reduction upwards) and $Cu_A$ (green, reduction downwards). The best three-exponential fit (lines) to the data (dots) yields time constants of 10, 150, and 800 $\mu$s. (*B*) The corresponding kinetics of membrane potential formation in vesicles inlaid with CcO. The fit (blue line) to the data (blue dots) with time constants from the optical measurements (10, 150, and 800 $\mu$s) requires one more component with a time constant of 2.6 ms. The relative amplitudes of the four phases are 12%, 42%, 30%, and 16% of total. The laser is fired at zero time.

we conclude that because the midpoint redox potential ($E_m$) of $Cu_A$ is 250 mV (14), the $E_m$ of heme *a* is ≈270 mV at this stage of the reaction, which is much lower than the "high asymptotic" $E_m$ reported from equilibrium redox titrations (14–18). From such titrations the $E_m$ of heme *a* is known to be pH-dependent, but on the microsecond time scale of electron equilibration between $Cu_A$ and heme *a* there is no coupled proton transfer (refs. 7, 19, and 20; see below). Therefore, the higher $E_m$ of heme *a* is not realized in this fast time domain, and the observed lower $E_m$ is the value for the case without the bound proton. Such a low "operational" $E_m$ of heme *a* during early electron equilibration with $Cu_A$ was also found previously for CcO from both bovine heart and *Paracoccus denitrificans* (21–23).

The intrinsic electron transfer rate between hemes *a* and $a_3$ has been found to be ~1 ns (24, 25) and is indeed expected to be much faster than the 10 $\mu$s transition because of the short heme-heme distance (26). Therefore, we may assume that the $Cu_A$/heme *a* pair is in electronic equilibrium with heme $a_3$ and $Cu_B$ on this time scale. Yet, no significant electron transfer to the $a_3/Cu_B$ site is observed in this phase based on the absence of absorption features due to reduction of these centers (Fig. 3*A*). From this fact, and the confidence level of ≈2%, follows that the $E_m$ values of heme $a_3$ and $Cu_B$ must be at least 100 mV lower than that of heme *a* at this early stage of the reaction.

Next follows a phase of electron transfer from heme *a* (and from $Cu_A$ with which heme *a* equilibrates on a 10 $\mu$s time scale) to the $a_3/Cu_B$ site with $\tau \sim 150$ $\mu$s (Figs. 2*A* and 3*A*). This phase consists of an ≈45% reoxidation of heme *a* from its previous reduction level, but $Cu_A$ appears to become completely reoxidized. Because of the low extinction of the $Cu_A$ absorbance, the noise level is now larger (see above), but the increase in absorbance at 820 nm during the following 800-$\mu$s phase (Fig. 2*A*) has a spectrum distinct from that of $Cu_A$ in the two earlier phases (data not shown), and must therefore be ascribed to other processes (see below). It has indeed been demonstrated that the near-infrared absorbance at 820 nm cannot be completely ascribed to $Cu_A$ (27).

This result allows us to conclude that the initial 70/30 electron distribution between heme *a* and $Cu_A$ after the 10 $\mu$s phase no longer prevails after the 150 $\mu$s phase. Assuming that the $E_m$ of $Cu_A$ remains unchanged, it is possible to conclude that the $E_m$ of heme *a* rises in this phase. The injected electron is now distributed ≈40% at heme *a* and 60% at the $a_3/Cu_B$ site. Recalling that the $E_m$ values of heme $a_3$ and $Cu_B$ were initially <170 mV (see above), it follows that the $E_m$ of the electron acceptor in the $a_3/Cu_B$ site is raised considerably in the 150 $\mu$s phase, and to a similar value as that of heme *a* ($\Delta E_m \approx 10$ mV). The simplest explanation for the observed rise in midpoint redox potentials of heme *a* and the $a_3/Cu_B$ site would be uptake of a proton to their vicinity, as discussed below.

In the third phase ($\tau \approx 800$ $\mu$s), heme *a* becomes fully oxidized (Figs. 2*A* and 3 *A* and *B*), which means that now the electron acceptor in the $a_3/Cu_B$ site has attained an $E_m$ much higher than those of all other sites. The ultimate electron acceptor in the $a_3/Cu_B$ site can be identified from the spectral difference between the final state *after*, and the state *before* electron injection (Fig. 3*B*). This spectrum shows that heme $a_3$ is not reduced, which identifies $Cu_B$ as the final electron acceptor. A 665-nm charge transfer band has been specifically attributed to a state where both heme $a_3$ and $Cu_B$ are oxidized (28), and its blue shift (Fig. 3*B*) can thus be unequivocally ascribed to reduction of $Cu_B$. Because reduction of $Cu_B$ is the only difference between the states before and after electron injection, the deviation of the 820 nm trace above the baseline in Fig. 2*A* can be ascribed to a small contribution of $Cu_B$ at this wavelength. Although not shown before, these results confirm the current belief that $Cu_B$ is the ultimate electron acceptor upon reduction of CcO by the first electron. However, the identity of the electron acceptor in the

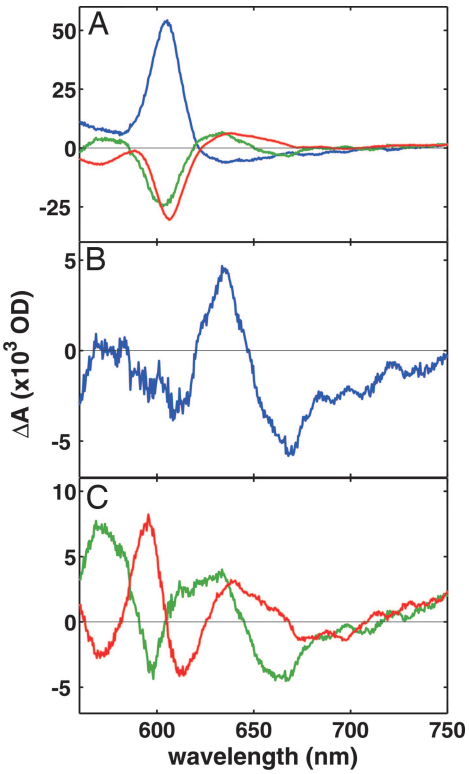


**Fig. 3.** Absorption spectra of reaction phases. (*A*) Kinetic absorption spectra of the 10-$\mu$s (blue), 150-$\mu$s (green), and 800-$\mu$s (red) phases. (*B*) Difference spectrum between the final product of the reaction minus the state before the laser pulse. (*C*) Difference spectra of the 150-$\mu$s (green) and 800-$\mu$s (red) reaction phases from which the contribution of heme *a* oxidation (see *A*) has been subtracted.

previous 150 $\mu$s phase is less obvious. The kinetic spectra of the individual 150- and 800-$\mu$s phases are different, best seen after subtracting the contribution from heme *a* oxidation (Fig. 3*C*). Absorption changes in the 560–620 nm region during the 150 $\mu$s phase are reversed in the 800-$\mu$s phase. It is therefore very likely that heme $a_3$ is the electron acceptor in the 150-$\mu$s phase, and that the 800-$\mu$s phase includes electron transfer from hemes *a* and $a_3$ to $Cu_B$.

We note here that full reoxidation of heme *a* in ≈1 ms, as described above, is not observed in all preparations of isolated CcO, although it is seen after electron injection into the F state (7). In many preparations, despite the "pulsing" procedure (see *Materials and Methods*), reduction of heme *a* is followed by reoxidation by only 50–80% within milliseconds. Such observations have also been made for isolated CcO from bovine heart and *Rhodobacter sphaeroides* (F. Millett and R. B. Gennis, personal communication). To assess which behavior is the native one, and thus more relevant with respect to function, we tested detergent-dispersed membrane preparations from *P. denitrificans* (see *Materials and Methods*), and here the kinetics showed full reoxidation of heme *a* in phases of ≈150 and 800 $\mu$s. We are thus confident that this behavior is the native reactivity of "pulsed" CcO, and it seems that many currently applied isolation procedures yield enzyme in which the fraction of the truly "$O_2$ pulsed" state is variable. At this time we do not have an explanation for this variation. Excess detergent or removal of phospholipids during enzyme isolation might be the cause, which requires further investigation.

**Charge Translocation.** Fig. 2*B* shows the kinetics of membrane potential formation after electron injection into CcO reconstituted into phospholipid vesicles. These kinetics are reasonably well fitted by the time constants of the three reaction phases observed spectroscopically, yielding relative amplitudes of 12%, 42%, and 30% of total. A fourth phase ($\tau \approx 2.6$ ms) has an amplitude of 16%, but no counterpart in the electron transfer kinetics. The full amplitude of membrane potential formation corresponds to translocation of two electrical charge equivalents across the dielectric per transferred electron (3, 13), one due to the convergence of electron transfer from the P-side with proton transfer from the N-side of the membrane (chemistry), and the other due to the pumped proton (Fig. 1). Therefore, the relative amplitudes of the four phases may be calibrated, yielding translocation of 0.24 (10-$\mu$s phase), 0.84 (150 $\mu$s), 0.60 (800 $\mu$s), and 0.32 (2.6 ms) charge equivalents, respectively, or translocation of a unit charge across these fractions of the membrane dielectric. These results may now be combined with the electron transfer data, as discussed below.

## Discussion

**The 10-$\mu$s Phase.** The events set into motion by electron injection into CcO are best understood as a temporally evolving cascade of equilibria (Fig. 4). After reduction of $Cu_A$, this site equilibrates with heme *a* in ≈10 $\mu$s, where 70% transfer of the injected electron from $Cu_A$ to heme *a* is reflected as translocation of 0.24 charges across the dielectric (see above). This value amounts to translocation of a unit charge across one third of the membrane per transferred electron (0.24/0.7 = 0.34), in good agreement with the relative dielectric distance between these centers (3, 7). Pure electron transfer from $Cu_A$ to heme *a* is hence fully accounted for electrometrically, which is consistent with the notion that it is not kinetically coupled to vectorial proton transfer as already concluded earlier on the basis of a lack of dependence of the rate of this reaction on pH, or solvent substitution with heavy water (cf. refs. 7, 19, and 20). This conclusion is also consistent with the initially low $E_m$ of heme *a* (see above).

**Evaluation of Redox Potentials.** Why does electron transfer to the $a_3/Cu_B$ site not occur immediately upon reduction of heme *a*? Electron tunneling between the hemes is intrinsically very fast (24, 25), but it is substantially delayed here, evidently due to linkage to proton transfer. The $E_m$ of the binuclear site is initially far lower than those of heme *a* and $Cu_A$, and we suggest that this difference precludes significant electron transfer for thermodynamic reasons. However, proton uptake in the 150-$\mu$s phase, revealed by the electrometric data, occurs simultaneously with a rise in the $E_m$ of heme $a_3$ to a value similar to that of heme *a* (revealed by absorption spectroscopy). The $E_m$ of heme *a* is also raised from its initial value of ≈270 mV, because no significant electron occupancy is observed at $Cu_A$ at this stage. The rise in the $E_m$ values of the two hemes can thus be attributed to proton uptake into their vicinity. Our data do not allow a quantitative assessment of these $E_m$ values for the 150-$\mu$s phase because there is no significant electron occupancy at $Cu_A$, the "standard" used for the 10-$\mu$s phase. However, we suggest that they might correspond to the "high-asymptotic" $E_m$ values of ≈360 mV observed in anaerobic redox titrations in equilibrium with protons (14, 17, 18).

In the 800-$\mu$s phase, which is also associated with electrogenic proton uptake, the $E_m$ of the ultimate electron acceptor ($Cu_B$; see above) must attain a value much higher than those of all other redox centers, because the latter have no electron occupancy after this phase (note that a 2% occupancy of heme *a* would have been detected; hence, the $E_m$ of $Cu_B$ must have risen to a value at least 100 mV higher than that of heme *a*).

**Assignment of the Proton Transfer Reactions.** The clear separation in time between the 150- and 800-$\mu$s phases of electron and proton transfer is of particular mechanistic interest. They con-

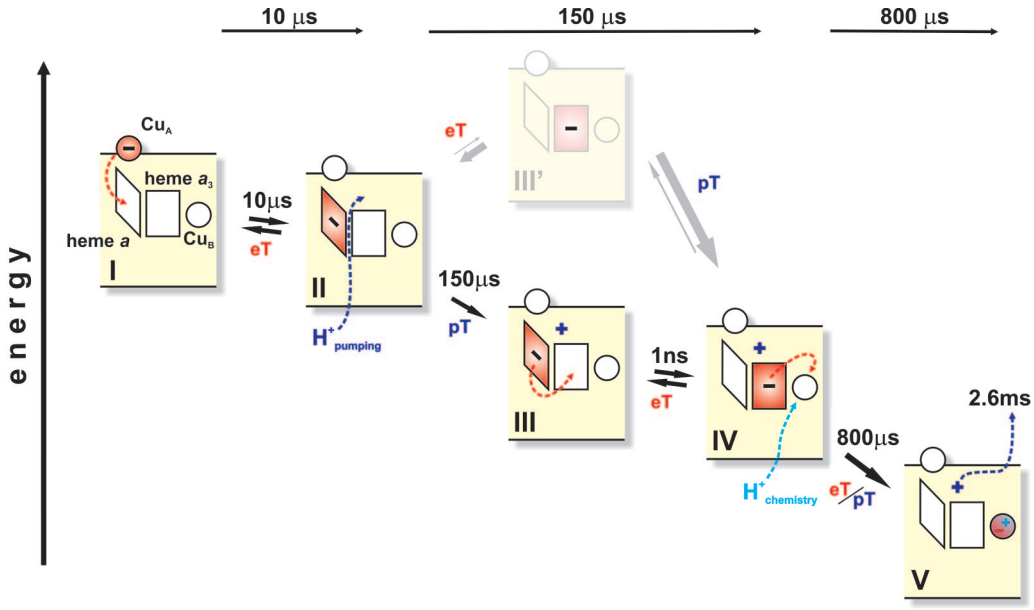


**Fig. 4.** Reaction scheme. The rhombus and square represent hemes *a* and $a_3$, respectively. The circle above heme *a* represents the $Cu_A$ site, and the circle next to heme $a_3$ represents $Cu_B$. The minus sign denotes the position of the photoinjected electron. The dark and light blue plus signs denote the pumped and substrate protons, respectively. Dashed arrows indicate electron and proton transfers during the next reaction step. eT, electron transfer; pT, proton transfer.

tribute to most of the membrane potential formation, of which only a small fraction can be due to remaining electron transfer between $Cu_A$ and heme *a*. Most of the electrogenicity must therefore be the result of two processes: uptake of the "substrate proton" from the N-side to the $a_3/Cu_B$ site, and uptake of the pumped proton (Fig. 1). These two reactions are well separated in time, as found earlier (cf. refs. 6 and 7), but which is due to uptake of the substrate proton, and which to the pumped proton? This is a key question, not least because previous work has been contradictory on this point. For example, Ruitenberg *et al.* (6) and Faxén *et al.* (29) have suggested that uptake of the substrate proton precedes uptake of the pumped proton, whereas others have presented evidence to the opposite (7, 30). Uptake of the substrate proton directly into the $a_3/Cu_B$ site is expected to raise the $E_m$ of that site much more than uptake of the pumped proton to a site located further away. If so, the assignment is straightforward: the 150-$\mu$s phase is due to uptake of the pumped proton from the aqueous N-side in a large fraction of the enzyme, and the 800-$\mu$s phase is mainly due to uptake of the substrate proton. This distinction leads to a plausible reaction scheme (Fig. 4).

**Reaction Scheme.** The injected electron initially equilibrates between $Cu_A$ and heme *a*, which are roughly equipotential at this stage. The reduction of heme *a* raises the $pK_a$ of a so far unidentified "pump site" above the heme groups (cf. refs. 7, 30, and 31), which takes up a proton in the 150-$\mu$s phase. The proton uptake raises the $E_m$ of both hemes, and allows electron equilibration between them in the same time window. The rise in the $E_m$ of heme $a_3$ is considerably larger than for heme *a* (see above), which suggests that the pump site is more closely linked to the former. Such a shared proton-binding site has long been predicted (16, 18) and finds clear functional significance here. As described for a photosynthetic reaction center (32), there are four possible states for a two-step mechanism describing such proton-coupled electron transfer, shown here by the upper and lower paths in Fig. 4. The rate may either be limited by proton or by electron transfer. Because of the very fast heme–heme electron tunneling time in CcO (24, 25), we may exclude those two reactions where electron transfer is rate-limiting. From the electron occupancies at the end of the 150-$\mu$s phase, we find that the protonated state with heme *a* reduced (Fig. 4, state III) is highly populated. The data excludes any significant population of the state where heme *a* is reduced without proton uptake (Fig. 4, state II), because of the absence of a measurable population of reduced $Cu_A$. Combining the optical and electrometric data further strengthens this conclusion. The charge translocation can be described as the sum of electron and proton transfers propagating perpendicular to the membrane plane. The 30% electron transfer from $Cu_A$ to heme *a* across one-third of the dielectric gives 0.1 charge equivalents (30% of 0.33). The location of the pump site is not known, but if we assume that it is at a relative dielectric distance *x* from the P-side of the membrane, proton transfer from the N-side to this site in the 150-$\mu$s phase adds $1 - x$ charge equivalents. Because we found the amplitude of this phase (proton + electron transfer) to be $\approx$0.84 charge equivalents, we may estimate *x* to be $\approx$0.25.

Our results favor a mechanism in which transfer of the pumped proton occurs before electron transfer to the binuclear center (contrast refs. 7 and 33), even though these two events have the same proton-limited kinetics. This finding is consistent with the conclusion by Brändén *et al.* (34) that protonation of the "pump site" controls this electron transfer, which is of considerable mechanistic interest because much previous work has stressed the importance of heme *a* in the proton pump mechanism (15, 18, 31, 33, 35–37). In the third phase, the substrate proton is transferred from the aqueous N-side, most likely to an $OH^-$ ligand of $Cu_B$ (38), which raises the $E_m$ of $Cu_B$ to a value much higher than that of all other centers. Hence, this step is essentially irreversible (Fig. 4) and provides the main driving force for the entire pump mechanism. Finally, the slowest step (2.6 ms), seen only electrometrically, is proposed to be due to release of the proton from the "pump site" to the P-side by electrostatic repulsion from uptake of the substrate proton (cf. refs. 31 and 36). The observed electrometric amplitude (one charge across $\approx$32% of the dielectric barrier) agrees reasonably well with the above estimate of the position of the pump site relative to the membrane, and the slow rate is consistent with the suggestion by Salomonsson *et al.* (39) that release of the pumped proton is the rate-limiting step.

Although our work goes some way toward a molecular un-

derstanding of the proton pump mechanism of CcO, some important details remain unsolved, e.g., the identity of the proton-accepting pump site above the hemes. The basis for transferring the first proton to this site, rather than to be consumed at the $a_3/Cu_B$ site, is also not fully understood although our data suggest a key role of heme *a* reduction. The observed thermodynamic effect of heme *a* reduction, i.e., the increase of the $pK_a$ of the pump site, is hardly sufficient to explain the destiny of the first proton because of the proximity of the $a_3/Cu_B$ site, whose $pK_a$ should also increase. The notion that reduction of heme *a* may also kinetically favor proton transfer to the pump site (36) may therefore still be valid.

## Materials and Methods

**Enzyme Preparation and Reconstitution into Phospholipid Vesicles.** CcO from *P. denitrificans* was isolated from bacterial membranes and purified as described (40), with the exception that the second Q-Sepharose column was replaced by a $Ni^{2+}$-NTA affinity chromatography column (see ref. 41 for details). In addition, the enzyme was washed and concentrated by using pressure dialysis (XM-50 membrane; Millipore, Bedford, MA) with 2 mM Tris·HCl (pH 8)/0.05% (wt/vol) dodecyl L-D-maltoside (DM)/20 mM aniline. The enzyme was reconstituted into vesicles by the Bio-Beads method (SM-2 adsorbent; Bio-Rad, Hercules, CA) as described (42), except that the concentration of CcO during reconstitution was increased to 6 $\mu$M.

Samples of detergent-dispersed *Paracoccus* membranes were prepared by solubilization of salt-washed membranes with 1% DM (Anatrace, Maumee, OH) in 20 mM Tris·HCl buffer (pH 7.8)/0.2 mM phenyl-methyl-sulfonyl-fluoride (PMSF), followed by ultracentrifugation (165,000 $\times$ *g*, 30 min), after which the supernatant was washed and concentrated by using pressure dialysis with 2 mM Tris·HCl (pH 8)/0.05% DM/20 mM aniline.

**Time-Resolved Measurement of Electric Potential Generation.** The development of electric potential across the vesicle membrane was monitored by an electrometric technique (43), as adapted for time-resolved experiments with CcO (44). Details of the sample preparation and the methodology can be found in refs. 8 and 42.

**Time-Resolved Spectrophotometric Measurements.** Time-resolved multiwavelength absorption changes were followed by using a home-constructed CCD-based instrument. A pulsed 150-W xenon arc lamp (Applied Photophysics, Surrey, U.K.) was used as the probe light source. Light from the lamp was passed although a glass filter (OG-550) and fibers to a three-syringes stopped-flow module (SFM-300; Bio-Logic, Grenoble, France) equipped with a fluorescence cuvette (TC-100/10F, optical path 10 mm) with the sample. The light was further directed to a Triax-180 compact imaging spectrograph (HORIBA Jobin Yvon, Edison, NJ), which delivers spectral imaging over a fast kinetic CCD matrix (DV420-UV-FK; Andor Technology, Belfast City, Ireland). The setup was operated by software written by N.B. and allows recording absorption change surfaces with a time resolution of 1–16 $\mu$s between the spectra. The reaction was initiated by laser flash-induced electron injection into the enzyme from RubiPy (Tris[2,2′-bipyridyl] ruthenium[II] chloride) (BrilliantB; Quantel, Les Ulis, France; frequency-doubled YAG, 532 nm, pulse energy = 120 mJ).

**Electron Injection.** To obtain the pulsed oxidized state for absorption measurements, a solution of 80 $\mu$M CcO in 2 mM Tris (pH 8)/0.05% DM/20 mM aniline/15 $\mu$M *N*,*N*,*N*′,*N*′-tetramethyl-*p*-phenylenediamine (TMPD) buffer was first made anaerobic on a vacuum line and then fully reduced by 1 mM potassium ascorbate. Then, anaerobic fully reduced CcO was mixed in the stopped-flow module with oxygen-saturated buffer (2 mM Tris (pH 8)/0.05% DM/20 mM aniline/400 $\mu$M RubiPy) resulting in oxidation CcO and formation of the pulsed state. Immediately after the mixing ($\Delta t$ = 5 ms), a laser flash initiated the electron injection.

In electrometry, the pulsed state was generated by oxidation of the fully reduced CO-bound CcO in vesicles. Fully reduced enzyme was produced by anaerobic reduction of CcO (4 mM Tris, pH 8/3.5 mg/ml glucose oxidase/50 $\mu$g/ml catalase/50 mM glucose/20 mM aniline/200 $\mu$M RubiPy/1 $\mu$M ruthenium hexa-amine) in a 1% CO atmosphere. The injection of oxygen-saturated buffer with aniline and RubiPy was performed through a needle directed toward the measuring membrane. The oxygen injection was followed by a series of flashes with 100-ms intervals. The first flash in this series photolyses CO off the enzyme and allows it to react with oxygen. The following flash induces photoinjection of an electron from RubiPy into the enzyme just oxidized (3).

We thank Virve Rauhamäki and Eija Haasanen for their invaluable help in enzyme purification. This work was supported by grants from the Sigrid Jusélius Foundation, Biocentrum Helsinki, and the Academy of Finland.

1. Gennis RB (2004) *Front Biosci* 9:581–591.
2. Michel H, Behr J, Harrenga A, Kannt A (1998) *Annu Rev Biophys Biomol Struct* 27:329–356.
3. Bloch D, Belevich I, Jasaitis A, Ribacka C, Puustinen A, Verkhovsky MI, Wikström M (2004) *Proc Natl Acad Sci USA* 101:529–533.
4. Mayo SL, Ellis WR, Jr, Crutchley RJ, Gray HB (1986) *Science* 233:948–952.
5. Nilsson T (1992) *Proc Natl Acad Sci USA* 89:6497–6501.
6. Ruitenberg M, Kannt A, Bamberg E, Fendler K, Michel H (2002) *Nature* 417:99–102.
7. Siletsky SA, Pawate AS, Weiss K, Gennis RB, Konstantinov AA (2004) *J Biol Chem* 279:52558–52565.
8. Jasaitis A, Verkhovskaya ML, Morgan JE, Verkhovsky MI, Wikström M (1999) *Biochemistry* 38:2697–2706.
9. Zaslavsky DL, Kaulen AD, Smirnova IA, Vygodina T, Konstantinov AA (1993) *FEBS Lett* 336:389–393.
10. Iwata S, Ostermeier C, Ludwig B, Michel H (1995) *Nature* 376:660–669.
11. Antonini E, Brunori M, Colosimo A, Greenwood C, Wilson MT (1977) *Proc Natl Acad Sci USA* 74:3128–3132.
12. Wilson MT, Peterson J, Antonini E, Brunori M, Colosimo A, Wyman J (1981) *Proc Natl Acad Sci USA* 78:7115–7118.
13. Verkhovsky MI, Jasaitis A, Verkhovskaya ML, Morgan JE, Wikström M (1999) *Nature* 400:480–483.
14. Gorbikova EA, Vuorilehto K, Wikström M, Verkhovsky MI (2006) *Biochemistry* 45:5641–5649.
15. Artzatbanov VY, Konstantinov AA, Skulachev VP (1978) *FEBS Lett* 87:180–185.
16. Moody AJ, Rich PR (1990) *Biochim Biophys Acta* 1015:205–215.
17. Blair DF, Ellis WR, Wang H, Gray HB, Chan SI (1986) *J Biol Chem* 261:11524–11537.
18. Wikström M, Krab K, Saraste M (1981) *Cytochrome Oxidase: A Synthesis* (Academic, London).
19. Oliveberg M, Brzezinski P, Malmström BG (1989) *Biochim Biophys Acta* 977:322–328.
20. Ruitenberg M, Kannt A, Bamberg E, Ludwig B, Michel H, Fendler K (2000) *Proc Natl Acad Sci USA* 97:4632–4636.
21. Kobayashi K, Une H, Hayashi K (1989) *J Biol Chem* 246:7976–7980.
22. Farver O, Einarsdottir O, Pecht I (2000) *Eur J Biochem* 267:950–954.
23. Farver O, Grell E, Ludwig B, Michel H, Pecht I (2006) *Biophys J* 90:2131–2137.
24. Verkhovsky MI, Jasaitis A, Wikström M (2001) *Biochim Biophys Acta* 1506:143–146.
25. Pilet E, Jasaitis A, Liebl U, Vos MH (2004) *Proc Natl Acad Sci USA* 101:16198–16203.
26. Page CC, Moser CC, Chen X, Dutton PL (1999) *Nature* 402:47–52.
27. Greenwood C, Hill BC, Eglinton DG, Thomson AJ (1983) *Biochem J* 215:303–316.
28. Mitchell R, Mitchell P, Rich PR (1991) *FEBS Lett* 280:321–324.
29. Faxén K, Gilderson G, Ädelroth P, Brzezinski P (2005) *Nature* 437:286–289.
30. Belevich I, Verkhovsky MI, Wikström M (2006) *Nature* 440:829–832.
31. Michel H (1999) *Biochemistry* 38:15129–15140.
32. Graige MS, Paddock ML, Bruce JM, Feher G, Okamura MY (1996) *J Am Chem Soc* 118:9005–9016.
33. Popovic DM, Stuchebrukhov AA (2004) *FEBS Lett* 566:126–130.
34. Brändén G, Brändén M, Schmidt B, Mills DA, Ferguson-Miller S, Brzezinski P (2005) *Biochemistry* 44:10466–10474.
35. Papa S, Capitanio N, Villani G (1998) *FEBS Lett* 439:1–8.
36. Wikström M, Verkhovsky MI, Hummer G (2003) *Biochim Biophys Acta* 1604:61–65.

37. Tsukihara T, Shimokata K, Katayama Y, Shimada H, Muramoto K, Aoyama H, Mochizuki M, Shinzawa-Itoh K, Yamashita E, Yao M, *et al.* (2003) *Proc Natl Acad Sci USA* 100:15304–15309.
38. Fann YC, Ahmed I, Blackburn NJ, Boswell JS, Verkhovskaya ML, Hoffman BM, Wikström M (1995) *Biochemistry* 34:10245–10255.
39. Salomonsson L, Faxén K, Ádelroth P, Brzezinski P (2005) *Proc Natl Acad Sci USA* 102:17624–17629.
40. Riistama S, Laakkonen L, Wikström M, Verkhovsky MI, Puustinen A (1999) *Biochemistry* 38:10670–10677.
41. Ribacka C, Verkhovsky MI, Belevich I, Bloch D, Puustinen A, Wikström M (2005) *Biochemistry* 44:16502–16512.
42. Verkhovsky MI, Tuukkanen A, Backgren C, Puustinen A, Wikström M (2001) *Biochemistry* 40:7077–7083.
43. Drachev LA, Jasaitis AA, Kaulen AD, Kondrashin AA, Liberman EA, Nemecek IB, Ostroumov SA, Semenov AYu, Skulachev VP (1974) *Nature* 249:321–324.
44. Verkhovsky MI, Morgan JE, Verkhovskaya ML, Wikström M (1997) *Biochim Biophys Acta* 1318:6–10.
45. Humphrey W, Dalke A, Schulten K (1996) *J Mol Graphics* 14:33–38.